Global dynamic scenarios in a discrete-time model of renewable resource exploitation: a mathematical study

Nonlinear Dynamics

Global dynamic scenarios in a discrete-time model of renewable resource exploitation: a mathematical study

--Manuscript Draft--

Manuscript Number:	NODY-D-20-00256
Full Title:	Global dynamic scenarios in a discrete-time model of renewable resource exploitation: a mathematical study
Article Type:	Original Research
Keywords:	Chaotic dynamics; Noninvertible maps; Milnor attractor; Global bifurcations; Complexity
Corresponding Author:	Anastasiia Panchuk Institue of Mathematics, NAS of Ukraine UKRAINE
Corresponding Author Secondary Information:	
Corresponding Author's Institution:	Institue of Mathematics, NAS of Ukraine
Corresponding Author's Secondary Institution:	
First Author:	Lorenzo Cerboni Baiardi
First Author Secondary Information:	
Order of Authors:	Lorenzo Cerboni Baiardi
	Anastasiia Panchuk
Order of Authors Secondary Information:	
Funding Information:	
Abstract:	We consider the two dimensional map introduced in Bischi et al. (2015) formulated as a model for a renewable resource exploitation process in an evolutionary setting. The global dynamic scenarios displayed by the model are not so often encountered in smooth two dimensional dynamical systems. We explain the occurrence of such scenarios at the light of the theory of noninvertible maps. Moreover, complex structures of basins of attraction of coexisting invariant sets are observed. We analyze such structures by examining stability properties of chaotic sets, in the case in which a non topological Milnor attractor is present. Stability changes of a chaotic set occur through global bifurcations (such as riddling and blowout) and are detected by means of the study of the spectrum of Lyapunov exponents associated with the set.
Order of Authors (with Contributor Roles):	Lorenzo Cerboni Baiardi (Investigation: Equal; Writing – original draft: Equal; Writing – review & editing: Equal)
	Anastasiia Panchuk (Investigation: Equal; Writing – original draft: Equal; Writing – review & editing: Equal)

Noname manuscript No.
(will be inserted by the editor)

Global dynamic scenarios in a discrete-time model of renewable resource exploitation: a mathematical study

Lorenzo Cerboni Baiardi · Anastasiia Panchuk

Received: date / Accepted: date

Abstract We consider the two dimensional map introduced in Bischi et al. (2015) formulated as a model for a renewable resource exploitation process in an evolutionary setting. The global dynamic scenarios displayed by the model are not so often encountered in smooth two dimensional dynamical systems. We explain the occurrence of such scenarios at the light of the theory of noninvertible maps. Moreover, complex structures of basins of attraction of coexisting invariant sets are observed. We analyze such structures by examining stability properties of chaotic sets, in the case in which a non topological Milnor attractor is present. Stability changes of a chaotic set occur through global bifurcations (such as riddling and blowout) and are detected by means of the study of the spectrum of Lyapunov exponents associated with the set.

Keywords Chaotic dynamics · Noninvertible maps · Milnor attractor · Global bifurcations · Complexity

1 Introduction

In the recent decades environmental problems arising from human activity have been drawing great attention of scientists from different research areas (e. g., [11, 4, 8] to cite a few). In particular, models describing exploitation of renewable natural resources have become rather popular (see, e. g., [25, 7, 16] and references therein). Within this stream of literature the contribution provided in [6] is placed. In that work, the authors consider a two dimensional map that is the discrete-time counterpart of the continuous-time dynamical system formulated in [16]. The map is a model for a renewable resource exploitation process (fishery), where the resource is renewed according to a logistic-type growth and where players choose between

L. Cerboni Baiardi
Department of Economics, Statistics and Finance, University of Calabria, Italy
E-mail: lorenzo.cerboni@unical.com

A. Panchuk
Institute of Mathematics, NAS of Ukraine, Kiev, Ukraine
E-mail: anastasiia.panchuk@gmail.com

two harvesting strategies according to the profit-driven evolutionary selection rule known as replicator dynamics (see [9,14]).

In the current paper we continue considering the nonlinear model proposed in [6]. We aim at explaining through mathematical and numerical analysis certain global dynamic scenarios that the model displays, some of which are quite unusually found in two dimensional smooth systems in discrete time. At first, we observe that the target two dimensional map is noninvertible and belongs to the class $Z_0 - Z_2$. Namely, a set in the state space of the map exists separating it into two regions, Z_0 and Z_2, whose points have no preimages and two preimages, respectively. Such a set is called *critical set* and it is the generalization in a higher dimensional framework of the notion of local maxima/minima of one dimensional maps (see, e. g., [13,1,22,2]). Critical sets play significant role in determining global phenomena, being responsible for qualitative changes of invariant sets and their basins of attraction. For instance, the critical set and its images can be used to obtain the boundaries of trapping regions or may cause occurrence of multiple connected or non-connected basins of attraction. Moreover, in certain configurations of parameters, the presence of a chaotic attractor is explained by detecting a mixed absorbing area, which is a trapping region delimited by portions of the critical sets of different rank and by segments of unstable sets of saddle cycles.

Furthermore, the evolutionary model here considered is characterized by the presence of a pair of one dimensional sets (more precisely, manifolds) that are invariant, i.e. mapped into themselves under the action of the map, and are located at the border of the region of feasible states. The dynamic processes taking place along such manifolds describe synchronization patterns where all players adopt the same strategy. We address the problem of synchronization achievement studying the transversal stability of the attractors embedded in the invariant manifolds, focusing on the nonstandard occurrence in which these attractors are chaotic sets. Through numerical computations of Lyuapunov exponents associated with the orbits nested in such chaotic sets, transversal stability changes can be highlighted. This analysis allows us to detect the occurrence of global bifurcation scenarios, such as riddling and blowout bifurcations. In detail, it may occur that, along certain bifurcation paths, the chaotic set can lose transversal stability, as it is meant in Lyapunov sense, turning into a so called non topological Milnor attractor [19]. The consequences of this bifurcation, called *riddling* bifurcation, are influenced by coexistence of multiple attractors. The long run convergence to synchronized dynamics can take place after a transient on-off intermittency (local riddling), where almost synchronized states are followed by asynchronous bursts, carrying the orbit far from the synchronization manifold. However, the fate of an orbit starting from initial conditions that are arbitrarily close to the synchronization manifold may also be different. Namely, the orbit diverges from the manifold to advance towards the coexisting inner attractor (global riddling). The explanation of these behaviors lies in the weak stability of the non topological Milnor attractor, being each point of its basin surrounded by points that belong to the basin of the other attractor. This circumstance determines complex structures of basins of attraction that are said to be riddled (see, e. g., [15,9]).

The paper is organized as follows. In Section 2 we introduce the map and recall its main properties. In Section 3 we report facts about fixed points, their possible bifurcations and the associated bifurcation conditions. Section 4 is devoted to studying nontrivial dynamics emerging when the internal fixed point E^* undergoes

a flip bifurcation. In particular, we describe a mixed chaotic area occurring after the respective period-doubling cascade (Sec. 4.2). In Section 5 coexistence of a Milnor attractor, located at the border of the feasible domain, and an internal attractor is studied. Section 6 concludes.

2 Preliminaries

In this section we recall briefly the original model setup and describe main properties of the map.

2.1 The model

Let us consider some target renewable resource (e. g., a particular kind of fish), whose available quantity at time t is denoted as $x(t)$. Suppose there are N agents (fishers) exploiting this resource choosing between two different technologies: an intensive (standard) one or environmentally friendly (ecological) one. The technologies are characterized by coefficients $q_1 > 0$ and $q_0 \in (0, q_1)$, respectively. The second variable $r(t) \in [0, 1]$ denotes the fraction of agents that use the standard technology during time period t, and hence, the fraction of agents $1 - r(t)$ use the ecological technology. Clearly, if $r(t) = 0$ ($r(t) = 1$) then all agents adopt ecological (standard) technology. It is also assumed that consumers buy the resource harvested by ecological (standard) technology at the constant price a_0 (a_1). Since ecological technology is supposed to be less efficient ($q_0 < q_1$), the respective resource should be more expensive, that is, $a_1 < a_0$.

In a discrete-time framework, the total quantity $x(t)$ of the resource is given by a model with non-overlapping generations (that is, a logistic-like equation) and the fraction $r(t)$ changes according to an exponential replicator dynamics [10,14]. In such a way, we get a two-dimensional map $F : \mathbb{R}^2 \ni (x, y) \to (x', r') \in \mathbb{R}^2$

$$F : \begin{cases} x' = \left(1 + \alpha - \dfrac{Na_0q_0}{2\gamma}\right) x - \dfrac{\alpha}{k}x^2 + \dfrac{N}{2\gamma}(a_0q_0 - a_1q_1)xr, \\ r' = r\left\{r + (1-r)\mathrm{e}^{\beta\left(\frac{a_0^2q_0 - a_1^2q_1}{4\gamma}x - \xi\right)}\right\}^{-1} \end{cases} \tag{1}$$

Clearly, the region of feasible states is $D_{\mathcal{F}} = \{(x, r) \ : \ x \geq 0, 0 \leq r \leq 1\}$. As for the remaining parameters, $\alpha > 0$ is the natural growth rate of the resource, $k > 0$ is its carrying capacity, i. e., the resource equilibrium level when there is no harvesting. The parameter $\gamma > 0$ represents a cost coefficient, so that, the larger is γ, the higher is the cost of harvesting. The intensity of choice $\beta \geq 0$ measures the reactiveness of agents, that is, for larger β greater fraction of agents change their minds in favor of the more profitable strategy. Finally, $\xi \in \mathbb{R}$ represents a policy parameter, regulating the profitability of one technology over the other. In fact, ξ equals the difference between fixed costs associated with the ecological technology and the fixed costs related to the standard technology. The values $\xi < 0$ mean that the fixed costs for intensive harvesting are higher, being the case assumed below.

2.2 Invariant sets and map reduction

As shown in [6], the map F has three invariant sets, namely, the lines $\mathcal{M} = \{(x,r) : x = 0\}$, $\mathcal{M}_0 = \{(x,r) : r = 0\}$ and $\mathcal{M}_1 = \{(x,r) : r = 1\}$, along which the dynamics is given by respective one dimensional restrictions. Orbits on $\mathcal{M}_i$, $i = 0, 1$, describe dynamic scenarios where players behave in the same way, all adopting either environmentally friendly technology (along $\mathcal{M}_0$), or the intensive technology (along $\mathcal{M}_1$). For this reason, we will refer to $\mathcal{M}_i$ as synchronization manifolds. At $\mathcal{M}_i$ the map F is reduced to $f_{r=i} : \mathbb{R} \ni x \to x' \in \mathbb{R}$ such that

$$x' = \left(1 + \alpha - \frac{Na_iq_i}{2\gamma}\right) x - \frac{\alpha}{k}x^2. \tag{2}$$

Each of the maps (2) is topologically conjugate to the logistic map $g : \mathbb{R} \ni z \to z' \in \mathbb{R}$, where

$$z' = \mu_i z(1 - z) \quad \text{with} \quad \mu_i = 1 + \alpha - Na_iq_i/(2\gamma), \tag{3}$$

through the homeomorphism $x = h(z) = k(2\gamma(1 + \alpha) - Na_iq_i)z/(2\gamma\alpha)$, that is, $f(h(z)) \equiv h(g(z))$. Hence, the map $f_{r=i}$ has two fixed points $x = 0$ and

$$x = \left(1 - \frac{Na_iq_i}{2\gamma\alpha}\right) k =: x_i^*. \tag{4}$$

The fixed point $x = 0$ is stable for $(Na_iq_i)/(2\gamma) - 2 < \alpha < (Na_iq_i)/(2\gamma)$. At $\alpha = (Na_iq_i)/(2\gamma)$ the points $x = x_i^*$ and $x = 0$ undergo the transcritical bifurcation, exchanging stabilities. For $(Na_iq_i)/(2\gamma) < \alpha < (Na_iq_i)/(2\gamma) + 2$, the fixed point $x = x_i^*$ is stable. And at $\alpha = (Na_iq_i)/(2\gamma) + 2$ it undergoes the flip bifurcation, implying appearance of a stable cycle of period 2 and the successive well-known bifurcation sequence along the line $r = i$ (see, e. g. [26,18,21]).

Along $x = 0$, the map F is reduced to $f_{x=0} : \mathbb{R} \ni r \to r' \in \mathbb{R}$ such that

$$r' = \frac{r}{r + (1 - r)\mathrm{e}^{-\xi\beta}}. \tag{5}$$

The map $f_{x=0}$ is increasing and has two fixed points $r = 0$ and $r = 1$. The former one is stable and the latter one is unstable for $\xi < 0$.

2.3 Critical lines

Before continuing investigation of the map dynamics recall that the map is noninvertible, so there are critical lines, which play an important role for global dynamics.

Recall that the notion of critical line (or set) is typical for noninvertible maps (see [13,22,1,2] to cite a few). *A critical line LC* is defined as a geometric locus of points in the phase space having at least two coincident preimages. These coincident preimages are located on the curve LC_{-1}, also referred to as the *curve of merging preimages*. In the case of the considered map F (being continuously differentiable) LC_{-1} is the set of points (x, r) such that[1]

$$\det DF(x, r) = 0. \tag{6}$$

[1] Note that in general LC_{-1} is only *included* in the set of points at which the determinant of the Jacobi matrix vanishes.

The equation (6) solved for r gives $LC_{-1} = \{(x, r) : r \in \mathbb{R}, x = \bar{x}\}$ with

$$\bar{x} = \bar{x}(r) = \frac{8k\gamma^2(1+\alpha) - 4k\gamma N(a_0q_0(1-r) + a_1q_1r)}{16\alpha\gamma^2 - \beta kN(a_0q_0 - a_1q_1)(a_0^2q_0 - a_1^2q_1)r(1-r)}. \tag{7}$$

The critical line (of rank 1) is then given as $LC_0 = F(LC_{-1}) := LC$, and the critical lines of higher rank k, $k \geq 2$, are the respective images $LC_{k-1} = F^{k-1}(LC)$.

The map F is of type $Z_2 - Z_0$, that is, phase points $(x, r) \in D_{\mathcal{F}}$ located to the right of the critical line $LC = F(LC_{-1})$ do not have preimages, while the points located to the left of LC have two preimages.

3 Trivial dynamics: fixed points

In this section we recall briefly the facts about feasibility and stability of fixed points of the map (1), described in detail in [6].

Clearly, the fixed points of one-dimensional restrictions $f_{x=0}$, $f_{r=0}$ and $f_{r=1}$ constitute also four fixed points of the two-dimensional map F. These points are the extinction fixed points $E_0^0(0,0)$ and $E_1^0(0,1)$ and the viable fixed points $E_0^*(x_0^*, 0)$ and $E_1^*(x_1^*, 1)$ under ecological and intensive harvesting, respectively. The points E_0^0 and E_1^0 always belong to the boundary $\partial D_{\mathcal{F}}$ of the feasible region, while E_0^* and E_1^* belong to $\partial D_{\mathcal{F}}$ if $x_0^* \geq 0$, $x_1^* \geq 0$ (otherwise they are not feasible). In addition, there exists the fifth fixed point $E^*(x^*, r^*)$, not related to the one-dimensional restrictions, with

$$x^* = \frac{4\xi\gamma}{a_0^2q_0 - a_1^2q_1}, \quad r^* = \frac{2\gamma\alpha(1-kx^*) - Na_0q_0}{N(a_1q_1 - a_0q_0)}. \tag{8}$$

The point E^* is feasible if $x^* > 0$ and $0 \leq r^* \leq 1$.

The fixed point E_0^0 is stable if $(Na_0q_0)/(2\gamma) - 2 < \alpha < (Na_0q_0)/(2\gamma)$ and $\xi\beta < 0$, while E_1^0 is stable if $(Na_1q_1)/(2\gamma) - 2 < \alpha < (Na_1q_1)/(2\gamma)$ and $\xi\beta > 0$. Note that at $\xi\beta = 0$ the points E_0^0 and E_1^0 undergo a particular kind of bifurcation related to the eigenvalue $+1$. Indeed, at $\xi\beta = 0$ the restriction $f_{x=0}$ becomes a linear identity function $f_{x=0} \equiv r$, and hence, for its fixed points $r = 0$ and $r = 1$ there occurs a degenerate bifurcation associated with the eigenvalue $+1$, at which the two points exchange stabilities. The same happens for the points E_0^0 and E_1^0 in the vertical direction. Namely, at $\xi\beta = 0$ any point $(0, r)$, $r \in \mathbb{R}$, is a fixed point of F with one multiplier being equal to $+1$.

The viable fixed point E_i^*, $i = 0, 1$, related to the case when all agents choose the same strategy, is stable if

$$\frac{Na_iq_i}{2\gamma} < \alpha < \frac{Na_iq_i}{2\gamma} + 2 \quad \text{and} \quad (-1)^i\xi < (-1)^i\frac{(a_0^2q_0 - a_1^2q_1)}{4\gamma}k\left(1 - \frac{Na_iq_i}{2\gamma\alpha}\right).$$

The condition $\alpha = (Na_iq_i)/(2\gamma)$ is related to the transcritical bifurcation along the line $r = i$, at which E_i^* collides with E_i^0 and becomes feasible, that is, for $\alpha > (Na_iq_i)/(2\gamma)$ there holds $x_i^* > 0$. The condition $\alpha = (Na_iq_i)/(2\gamma) + 2$ is associated with the flip bifurcation, due to which a 2-cycle on the line $r = i$ appears. When the third equality holds

$$\xi = \frac{(a_0^2q_0 - a_1^2q_1)}{4\gamma}k\left(1 - \frac{Na_iq_i}{2\gamma\alpha}\right),$$

there occurs the transcritical bifurcation for the points E_i^* and E^*.

Finally, the point E^* is stable if the following three inequalities hold:

$$\left(\frac{Na_0q_0}{2\gamma} - B\right)\left(\frac{Na_1q_1}{2\gamma} - B\right)\xi\beta > 0, \tag{9}$$

$$\left(\frac{Na_0q_0}{2\gamma} - B\right)\left(\frac{Na_1q_1}{2\gamma} - B\right)\xi\beta + 2\left(2 - \alpha A\right)\frac{N(a_1q_1 - a_0q_0)}{2\gamma} > 0, \tag{10}$$

$$\left(\frac{Na_0q_0}{2\gamma} - B\right)\left(\frac{Na_1q_1}{2\gamma} - B\right)\xi\beta - \alpha A\frac{N(a_1q_1 - a_0q_0)}{2\gamma} < 0, \tag{11}$$

where

$$A = \frac{4\xi\gamma\alpha}{(a_0^2q_0 - a_1^2q_1)k}, \quad B = \alpha(1 - A).$$

The equalities in (9), (10), and (11) are related to the transcritical, flip, and Neimark-Sakker bifurcations of E^*, respectively.

To proceed we have to choose the parameter space section, which is not a simple task taking into account that there are ten parameters. Note that the inequalities (9), (10), and (11) are most easily solved with respect to ξ or β. Recall that the parameter ξ represents governmental policies regulating the prevalence of one technology over the other, in particular, it includes fixed taxes imposed. On the other hand, β measures the reactiveness of agents controlling how quickly the agents adopt to the changes on the market. Therefore, the choice of (ξ, β) plane as the main parameter space section seems reasonable.

A typical bifurcation diagram in the (ξ, β) parameter plane can be different depending on the values of the other eight parameters. Two examples are presented in Figs. 1(a),(b). In the panel (a), for larger value of $\alpha = 5.5$, one can see that for values of ξ closer to zero there is a periodicity region associated with an attracting cycle $\mathcal{O}_2^1$ located on the invariant line $r = 1$. It undergoes a transcritical bifurcation at $\xi \approx -0.17325$ (the related line $\kappa_{\mathcal{O}_2^1,\mathcal{O}_2}$ is shown blue) becoming a saddle, while the other 2-cycle $\mathcal{O}_2$ becomes stable entering the feasible region $D_{\mathcal{F}}$ from above. Further, due to a flip bifurcation (the related curve η_{E^*} is shown red) the internal fixed point E^* attains stability, and then it becomes an unstable focus through a Neimark-Sakker bifurcation (the related curve ζ_{E^*} is shown green). For smaller $\alpha = 3.39203$ (Fig. 1(b)), the fixed point E^* becomes stable due to a transcritical bifurcation (the corresponding line κ_{E^*,E_0^*} is shown blue) colliding with E_0^*, at the line $r = 0$, and entering $D_{\mathcal{F}}$ from below. Then it can lose stability through a flip or a Neimark-Sakker bifurcation (the corresponding curves η_{E^*} and ζ_{E^*} are shown again by red and green lines, respectively). Below we consider in detail this second parameter space section.

4 Nontrivial dynamics

In this section we describe dynamics different from fixed points. Below we observe that the dynamics of the map is rather rich, including cyclic closed invariant curves, mixed chaotic areas and Milnor attractors.

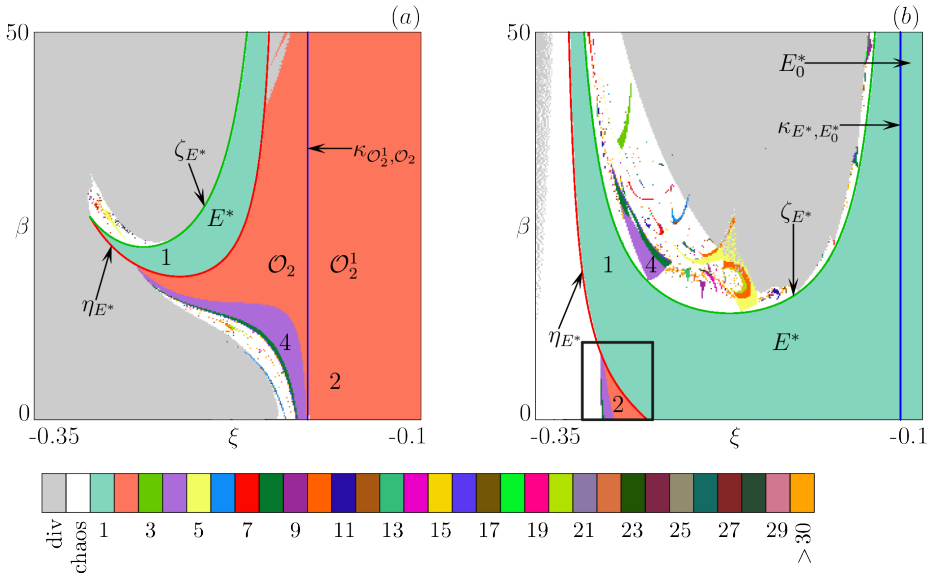

Fig. 1 Color coded 2D bifurcation diagrams in (ξ, β) parameter plane with different colors corresponding to different periods. (a) $\alpha = 5.5$, (b) $\alpha = 3.39203$. The other parameters are $a_0 = 1.973, a_1 = 1.91, q_0 = 0.1013, q_1 = 0.404, \gamma = 1.875, N = 15, k = 3$.

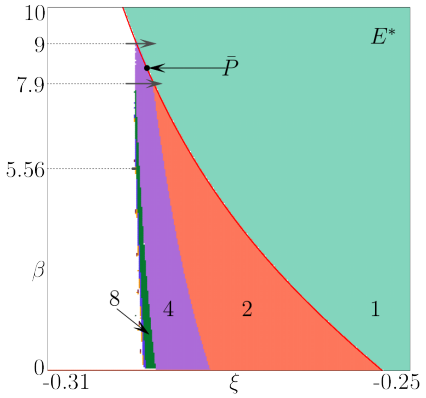

Fig. 2 2D bifurcation diagram in (ξ, β) parameter plane for $\alpha = 3.39203$ showing the region near the flip bifurcation of E^*. The other parameters and the meaning of colors are as in Fig. 1.

4.1 Dynamics near flip bifurcation of E^*

In Fig. 2 we see the rectangular area marked in Fig. 1(b), related to the period doubling cascade emerging after the flip bifurcation of E^*. The black point marks the parameter point $\bar{P} = (\xi, \beta)$ with $\xi \approx -0.29355$, $\beta \approx 8.33$, at which the type of the flip bifurcation changes from supercritical (below $\bar{P}$) to subcritical (above $\bar{P}$).

At the first site, the diagram looks strange, since intuitively one expects that the regions related to period-doubling sequence should all converge to the point $\bar{P}$, and they do not (except for the region related to the stable 2-cycle). To understand

this occurrence in detail, we plot in Fig. 3, 1D diagrams versus ξ along two arrows marked in Fig. 2. The gray stripes denote the attractor at the line $r = 0$, while blue and green colors are related to two different attractors located in interior of $D_{\mathcal{F}}$. In panels (a), (c) for $\beta = 7.9$, one can see that the stable 2-cycle $\mathcal{O}_2$ appears due to the (supercritical) flip bifurcation of E^* and then disappears for smaller ξ due to the fold bifurcation. The related complementary saddle cycle $\tilde{\mathcal{O}}_2$ is shown by solid red line. Hence, the periodicity region related to $\mathcal{O}_2$ is confined by three borders, namely, the curve related to the flip bifurcation of E^*, the curve related to the flip bifurcation of $\mathcal{O}_2$, and the curve related to the fold bifurcation of $\mathcal{O}_2$ and $\tilde{\mathcal{O}}_2$.

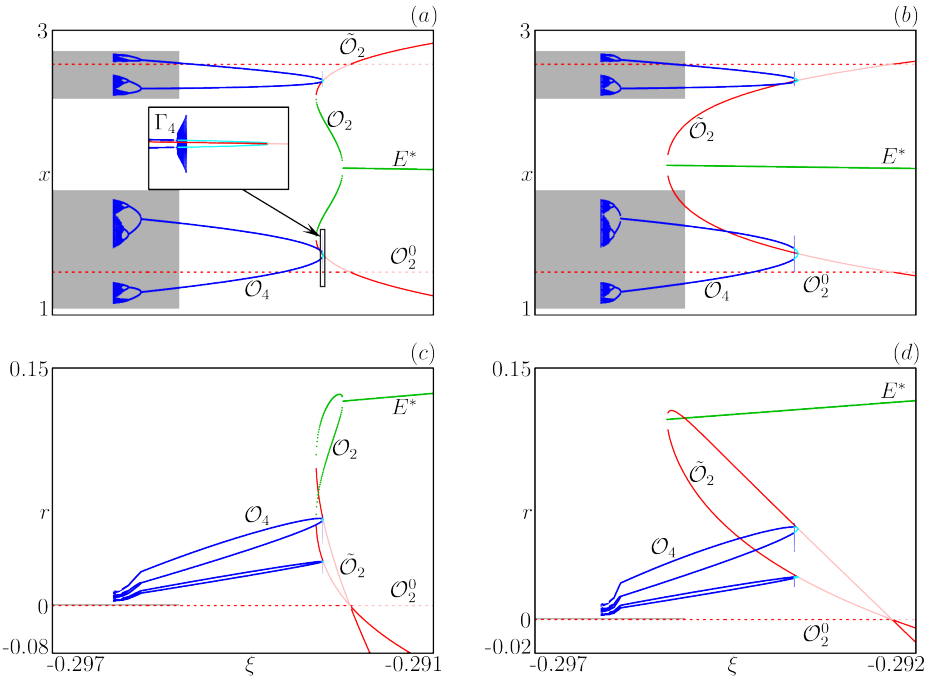

Fig. 3 1D bifurcation diagrams corresponding to the two arrows marked in Fig. 2. Green and blue denote 2 orbits related to different initial conditions, red color denotes the saddle 2-cycle, which collides with stable 2-cycle due to fold bifurcation (a, c) $\beta = 7.9$; (b, d) $\beta = 9$.

The flip bifurcation of $\mathcal{O}_2$ implies appearance of the stable 4-cycle $\mathcal{O}_4$. However, if the 2-cycle disappears due to fold bifurcation at $\theta_{\mathcal{O}_2,\tilde{\mathcal{O}}_2}$ or if it does not exist (in case of subcritical flip bifurcation of E^*), the cycle $\mathcal{O}_4$ must appear due to another bifurcation. For explaining this let us follow the cycle $\tilde{\mathcal{O}}_2$ starting from the value of ξ for that it is located below the line $\mathcal{M}_0$ and is a saddle. With decreasing ξ, it becomes an unstable node (shown pink) due to a transcritical bifurcation colliding with the unstable 2-cycle $\mathcal{O}_2^0 \subset \mathcal{M}_0$ (shown by dashed pink line, being unstable, and red line, being saddle). Then $\tilde{\mathcal{O}}_2$ undergoes a flip bifurcation becoming again a saddle while an unstable node 4-cycle $\mathcal{O}_4$ appears (shown by cyan line). Eventually $\mathcal{O}_4$ becomes an unstable focus, being surrounded by four cyclic invariant curves

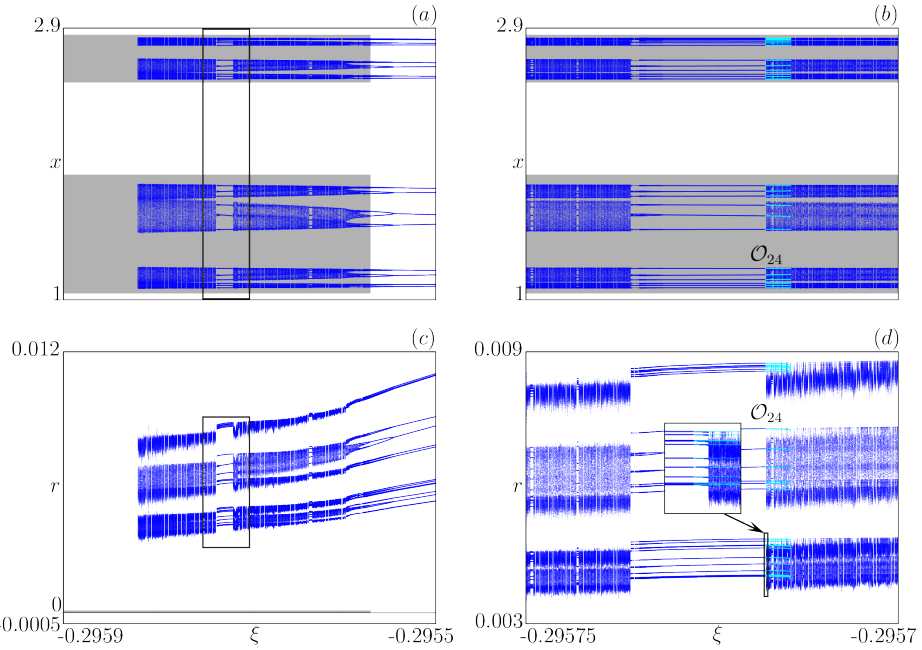

Fig. 4 1D diagram for $\beta = 5.56$ (the respective path is marked in Fig. 2 by a short black line segment).

Γ_4 and then becomes stable due to a Neimark-Sakker bifurcation. For a certain range of ξ there are two internal attractors coexist, whose basins of attraction are separated by the stable set of the saddle $\tilde{\mathcal{O}}_2$. For completing the description of the presented bifurcation scenario, we mention that with *increasing* ξ the invariant curves Γ_4 undergo a sequence of bifurcations, first becoming pleated and then transforming to a chaotic attractor $\mathcal{Q}$ that disappears due to a boundary crisis.

4.2 Mixed chaotic area

With decreasing ξ the aforementioned 4-cycle $\mathcal{O}_4$ loses stability due to the flip bifurcation and the standard period-doubling cascade is observed (see, e. g., Figs. 2 and 3). Eventually asymptotic dynamics becomes nonregular. To describe the related attractor in detail let us fix $\beta = 5.56$. In Fig. 4 the respective 1D bifurcation diagram is shown, where gray stripes denote the attractor at the line $\mathcal{M}_0$. Cyan line denotes the unstable cycle $\mathcal{O}_{24}$ mentioned below.

In Fig. 5 we plot state space with the related 8-piece chaotic attractor $\mathcal{Q}_8$ for $\xi = -0.29571$. There are also shown two saddle cycles $\mathcal{O}_4$ and $\mathcal{O}_8$ together with some part of their unstable sets $W^u(\mathcal{O}_4)$ and $W^u(\mathcal{O}_8)$. Noteworthy, the stable multipliers of both cycles are $0 < \mu_4^s < 1$, $0 < \mu_8^s < 1$. Clearly, $W^u(\mathcal{O}_4)$ and $W^u(\mathcal{O}_8)$ asymptotically approach $\mathcal{Q}_8$, and the structure of these sets is rather complex due to infinitely many pleats and self-intersections.

Let us define the domain $\Delta = \cup_{i=1}^4 \Delta_i$ confined by the critical lines LC_n, $n = 0, \ldots, 7$, and the appropriate segments of unstable sets $W^u(\mathcal{O}_4)$ and $W^u(\mathcal{O}_8)$.

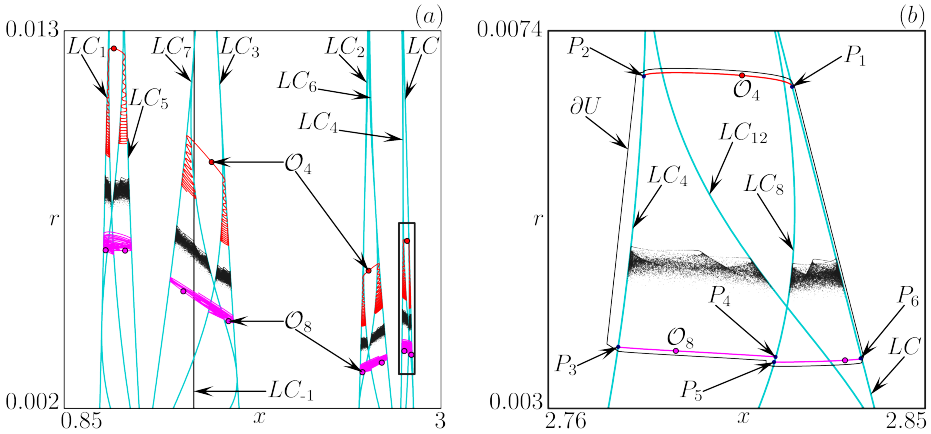

Fig. 5 State space for $\beta = 5.56$, $\xi = -0.29571$. The stable cycles $\mathcal{O}_4$ and $\mathcal{O}_8$ together with their unstable sets are shown red and magenta, respectively. In (b) the rectangular area marked in (a) is shown enlarged. The black line contours the neighborhood $U = U(\Delta_1)$.

The domains Δ_i are cyclically mapped one into another, that is, $F(\Delta_i) \subseteq \Delta_{i+1}$, $i = 1, 2, 3$, $F(\Delta_4) \subseteq \Delta_1$. For instance, the domain Δ_1 is shown in Fig. 5(b). Its boundary is a closed contour $\partial\Delta = (P_1P_2P_3P_4P_5P_6P_1)$, where the points P_i are intersections of LC, LC_4, LC_8 and $W^u(\mathcal{O}_4)$, $W^u(\mathcal{O}_8)$. In fact, Δ_1 is the absorbing area of mixed type for F^4. Indeed (see, e. g., [22] for definition),

1. $F^4(\Delta_1) \subset \Delta_1$,
2. there exists a neighborhood $U = U(\Delta_1)$ such that $F^4(U) \subset U$ and almost all points $(x, r) \in U \backslash \Delta_1$ (except for the points belonging to stable sets $W^s(\mathcal{O}_4)$, $W^s(\mathcal{O}_8)$) have finite rank image in the interior of Δ_1 (the boundary ∂U of the neighborhood U is shown in Fig. 5(b) by black line),
3. the boundary $\partial\Delta_1$ consists of segments of critical lines and unstable sets of saddle cycles.

Similarly, every domain Δ_i, $i = 2, 3, 4$, is the mixed absorbing area for F^4. It means that $\Delta = \cup_{i=1}^4 \Delta_i$ is the mixed absorbing area for F. Moreover, it is also known that if Δ is the mixed absorbing area, then its image $F(\Delta)$ is the mixed absorbing area as well, according to the Proposition 4.2′ from [22, p. 208]. Hence, either (i) there exists a finite M such that $F^M(\Delta)$ is invariant, that is, $F^{M+1}(\Delta) = F^M(\Delta)$, or (ii) $\cap_{i=1}^{\infty} F^i(\Delta)$ is invariant. Anyway, the invariant mixed absorbing area so obtained represents the chaotic attractor $\mathcal{Q}_8$.

Further, let us turn back to the 1D diagram shown in Fig. 4. For the value of $\xi \approx -0.2957177$ the attractor suddenly shrinks (see the inset in Fig. 4(d)). In Fig. 6(a) the part of the state space for $\xi = -0.295715$ is shown, where one can see the rightmost piece (the closest to LC) of the chaotic attractor $\mathcal{Q}_8$. Inside $\mathcal{Q}_8$ the are two cycles marked, namely, the unstable node cycle $\mathcal{O}_{24}$ (cyan points) and the saddle cycle $\tilde{\mathcal{O}}_{24}$ (red points), which appeared for larger ξ due to a flip bifurcation ($\mathcal{O}_{24}$ is also shown in Fig. 4 by cyan line). With decreasing ξ, due to an interior crisis, the cycle $\tilde{\mathcal{O}}_{24}$ together with its unstable set $W^u(\tilde{\mathcal{O}}_{24})$ "detaches" from $\mathcal{Q}_8$, which suddenly decreases in size and splits into 24 pieces. The case right after this bifurcation is depicted in Fig. 6(b), where $W^u(\tilde{\mathcal{O}}_{24})$ is shown by red

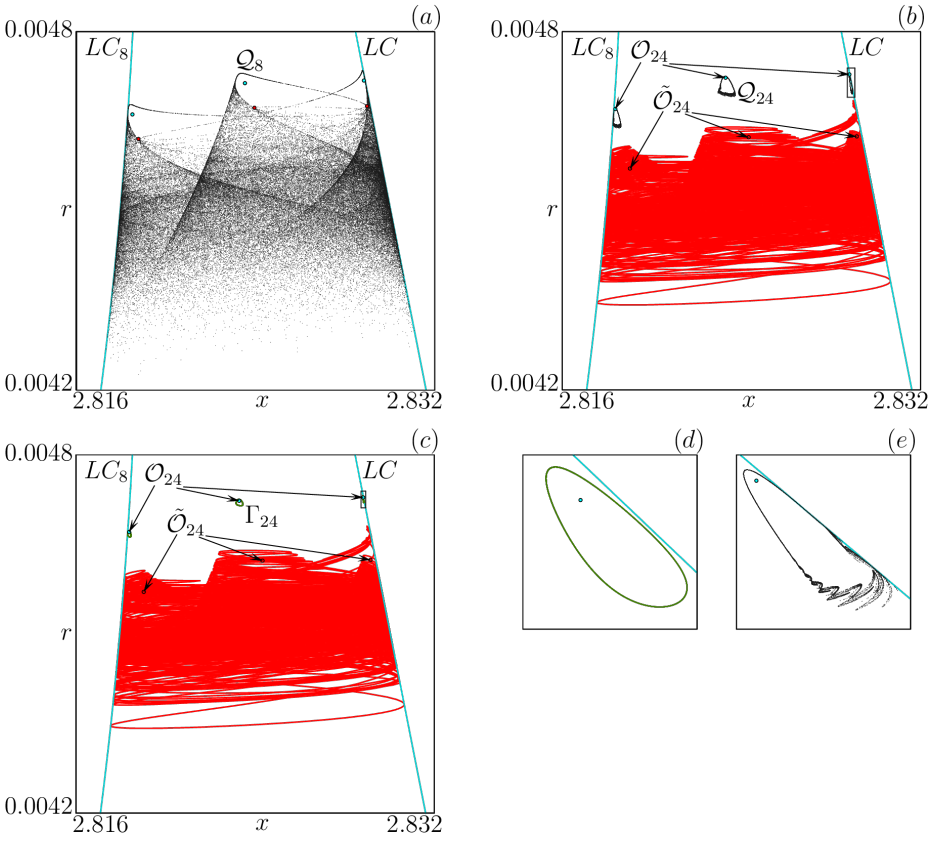

Fig. 6 State space for $\beta = 5.56$ and (a) $\xi = -0.295715$, (b) $\xi = -0.29571771307$, (c) $\xi = -0.29571775$; (d) and (e) show the rectangular areas marked in (c) and (b), respectively. Red and cyan points mark the saddle and the unstable cycles $\tilde{\mathcal{O}}_{24}$ and $\mathcal{O}_{24}$, respectively.

line. When ξ is decreased further, 24-piece chaotic attractor $\mathcal{Q}_{24}$ is transformed into 24-cyclic invariant curves Γ_{24}, now surrounding the unstable focus $\mathcal{O}_{24}$ (see Fig. 6(c)). Eventually, $\mathcal{O}_{24}$ undergoes a Neimark-Sakker bifurcation and becomes stable with succeeding period-doubling cascade that finally leads to the chaotic attractor $\mathcal{Q}_8$ again.

This particular bifurcation scenario is typical for considered range of the parameter ξ and is repeated for cycles of different periods. For example, at $\xi \approx -0.29563$ similar periodicity window corresponding to period 40 exists, where the same bifurcation sequence is observed (this window is distinguishable in Figs. 4(a), (c)).

5 Routes to synchronization

In this section we address the problem of reaching synchronization, namely, we ask when initial conditions that are placed out of $\mathcal{M}_i$ exist, whose iterations converge in the long run to $\mathcal{M}_i$. From an interpretative point of view, this corresponds to the

achievement of behavioral homogeneity among players, given initial configurations of the population characterized by behavioral heterogeneity. From a mathematical perspective, we search conditions for which

$$\lim_{t\to+\infty} F^t(x_0, r_0) \in \mathcal{M}_i, \;\; i = 0, 1,$$

holds for some initial condition $(x_0, r_0) \notin \mathcal{M}_i$. Therefore, the asymptotic dynamics consists of synchronization patterns governed by one-dimensional restrictions $f_{r=i}$ on $\mathcal{M}_i$.

If we denote by A_i the attractor of the restriction $f_{r=i}$, the problem of convergence to $\mathcal{M}_i$ can be addressed by studying the stability of attractors A_i with respect to perturbations transverse to $\mathcal{M}_i$.[2] To this end, we will compute the transverse Lyapunov exponents associated with orbits $\tau_i(x_0) \subseteq A_i$, with initial condition $x_0 \in A_i$. Denoting the eigenvalue of the Jacobian matrix of F at $x \in \mathcal{M}_i$ corresponding to eigendirection transverse to $\mathcal{M}_i$ by $\nu_{i,\perp}(x)$, the transverse Lyapunov exponent related to the orbit $\tau_i(x_0)$ is defined by

$$\Lambda_\perp(\tau_i(x_0)) = \lim_{T\to\infty} \frac{1}{T} \sum_{t=0}^{T} \ln|\nu_{i,\perp}(x_t)|.$$

For sake of brevity, we will omit the explicit dependence of Lyapunov exponents on the orbits to which they are related, when no ambiguity is possible. If x_0 belongs to a period k-cycle $\mathcal{O}_k$, then the transverse Lyapunov exponent associated with $\mathcal{O}_k$ is $\Lambda_\perp = \ln|\prod_{j=1}^{k} \nu_{i,\perp}(x_j)|$ and a sufficient condition for the transverse stability (instability) of the cycle is that $\Lambda_\perp < 0$ (> 0). Clearly, this is equivalent to the condition expressed in terms of the modulus of the transverse eigenvalue of $\mathcal{O}_k$, that is $|\prod_{j=1}^{k} \nu_{i,\perp}(x_j)| < 1$ (> 1).

A different and non standard situation is encountered when the attractor A_i is a chaotic set. When this is the case, the transverse Lyapunov exponent corresponding to a generic aperiodic trajectory embedded in A_i is not sufficient to fully characterize the stability property of the attractor. In detail, for a generic aperiodic orbit in A_i, the associated exponent $\Lambda_\perp$ is the so called *natural transverse Lyapunov exponent*, where by the term "*natural*" we mean the Lyapunov exponent related to the Sinai-Bowen-Ruelle measure. However, since infinitely many periodic cycles of any period are nested in the chaotic set A_i, a spectrum of transverse Lyapunov exponents can be defined (see [5,9]):

$$\Lambda_\perp^{\min} \leq \cdots \leq \Lambda_\perp^{\text{nat}} \leq \cdots \leq \Lambda_\perp^{\max}.$$

The natural transverse Lyapunov exponent of A_i is denoted by $\Lambda_\perp^{\text{nat}}$ and it accounts for the average transverse attractiveness of A_i, since it provides a "weighted balance" among transversely repelling and attracting cycles nested in A_i (see [23]). When all such cycles are transversely attractive, in which case $\Lambda_\perp^{\max} < 0$, A_i is transversely stable in Lyapunov sense for the two dimensional map F. Differently, when only some cycles are transversely unstable while the set A_i remains transversely attractive on average, in which case $\Lambda_\perp^{\max} > 0$ and $\Lambda_\perp^{\text{nat}} < 0$, then the set A_i is a so called non topological Milnor attractor, namely an attractor with a basin of positive Lebesgue measure in the two dimensional phase space (see [20]). The

[2] An attractor A_i of the restriction $f_{r=i}$ is stable with respect to perturbations along $\mathcal{M}_i$.

transition from the asymptotic stability of A_i to the weaker stability in Milnor sense, which corresponds to the transition of $\Lambda_\perp^{\max}$ from negative to positive values, determines the occurrence of a global bifurcation known as "*riddling*". (see [15]). Another possible occurrence is that the transversely unstable periodic orbits embedded into A_i have a greater weight as compared with the stable ones, in which case $\Lambda_\perp^{\text{nat}}$ is positive. In this event, the set A_i is a so called *chaotic saddle* and its basin is a set of points of zero measure in the plane. The transition of $\Lambda_\perp^{\text{nat}}$ from negative to positive values, after which the Milnor attractor A_i turns into a *chaotic saddle*, determines the occurrence of a second global bifurcation known as "*blowout*" (see [9]). Finally, when all cycles embedded in A_i are transversely repelling, in which case $\Lambda_\perp^{\min} > 0$ holds, the set A_i is a so called *chaotic repellor* with basin of attraction made up by points of A_i only (see [9]).

In the case of synchronization manifold $\mathcal{M}_0$, the transverse Lyapunov exponent of an orbit $\tau(x_0) = \{x_t = F_0^t(x_0),\ t \geq 0\} \subseteq A_0$ results

$$\begin{aligned}\Lambda_\perp(\tau(x_0)) &= \lim_{t\to\infty} \frac{1}{T}\sum_{t=1}^{T} \log|\nu_{0,\perp}(x_t)| \\ &= \beta\left(-\frac{a_0^2 q_0 - a_1^2 q_1}{4\gamma}\lim_{t\to\infty}\frac{1}{T}\sum_{t=1}^{T} x_t + \xi\right). \end{aligned} \tag{12}$$

We focus on the case in which A_0 is a chaotic set. This occurs when the parameter μ_0 of the respective conjugated logistic map (3) attains the values μ_0^j, with $j = 0, 1, 2...$, at which the first homoclinic bifurcation of a cycle of period 2^j occurs, causing the reunion of 2^{j+1} chaotic intervals into 2^j chaotic intervals, merging at the repelling periodic points of the cycle of period 2^j (see, e. g., [12,21]). The set A_0 is then given by the union of the 2^j cyclic chaotic intervals. For instance, the first of such values is $\mu_0^0 = 3.678573510428...$, at which A_0 is a chaotic interval that results from merging of two chaotic intervals at the repelling fixed point x_0^* of map $f_{r=0}$ that undergoes its first homoclinic bifurcation.

Note that the aggregate parameter μ_0 can be adjusted by suitable choices of parameters α, a_0, q_0, N and γ that completely determine the dynamics along $\mathcal{M}_0$. Moreover, the restriction $f_{r=0}$ does not depend on the parameters a_1, q_1, β and ξ and their variations keep the nature and properties of the attractor A_0 unchanged. Due to this circumstance, a_1, q_1, β and ξ are called *normal parameters*. However, such normal parameters influence the transverse stability of an orbit on $\mathcal{M}_0$, as it is clear from the analytic expression of the transverse Lyapunov exponent given in (12). The presence of normal parameters gives us the chance to fix the value of μ_0 such that the attractor A_0 is a chaotic set and to illustrate how its transverse stability smoothly changes along bifurcation paths that involve variations in normal parameters. In the following illustrative simulations, we will fix the value of the parameter μ_0 at the second element of the sequence $\mu_0^1 = 3.59257218410697...$. In this event, the attractor $A_0 = A_0^{(1)} \cup A_0^{(2)}$ of $f_{r=0}$ represents two cyclic chaotic intervals $A_0^{(1)}$ and $A_0^{(2)}$ obtained by the merging of 4 cyclic chaotic intervals when the unstable period-2 cycle of $f_{r=0}$ undergoes the first homoclinic bifurcation.

Figure 7 shows how the natural transverse Lyapunov exponent $\Lambda_\perp^{\text{nat}}$ varies at increasing values of ξ. In the same figure, the exponent $\Lambda_\perp^{\text{nat}}$ is paired up with the transverse Lyapunov exponent $\Lambda_\perp(\mathcal{O}_4)$ associated with the cycle $\mathcal{O}_4$ of period

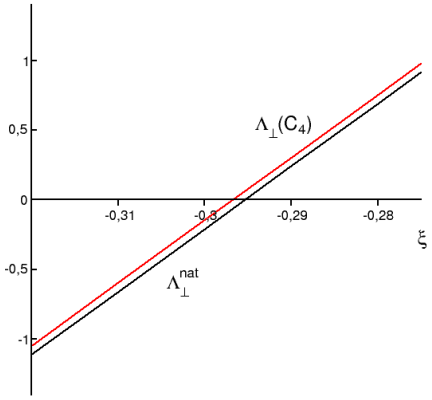

Fig. 7 Transverse natural Lyapunov exponent $\Lambda_\perp^{\rm nat}$ (black) associated with the generic aperiodic orbit embedded in the chaotic set A_0 and transverse Lyapunov exponent $\Lambda_\perp(\mathcal{O}_4)$ (red) associated with the period 4-cycle $\mathcal{O}_4 \subset A_0$ as ξ increases. Other parameters are $a_0 = 1.973$, $q_0 = 0.1013$, $a_1 = 1.91$, $q_1 = 0.404$, $\gamma = 1.875$, $N = 15$, $\alpha = 3.39203$, $k = 3$ and $\beta = 45$. Note that $\mu_0 = 1 + \alpha - Na_0q_0/(2\gamma) = \mu_0^1$.

4 embedded in A_0, which provides a lower estimate of $\Lambda_\perp^{\max}$. Clearly, when ξ is sufficiently low, all the cycles embedded in A_0 are transversely attracting. This claim follows from the analytic expression (12) of $\Lambda_\perp$, where the first term inside the parentheses attains positive[3] and finite values when computed along a periodic orbit. Hence, a value of ξ exists such that $\Lambda_\perp^{\max} < 0$, in which case A_0 is stable in Lyapunov sense. This situation is represented in Fig. 8(a), where the basins of attraction of A_0 (white points) and of the stable fixed point E^* (magenta points) are depicted in the phase space. In that simulation, the value $\xi = -0.32$ is conjectured to be sufficiently low to have $\Lambda_\perp^{\max} < 0$. The increase of ξ beyond the threshold at which $\Lambda_\perp^{\max} = 0$ causes riddling bifurcation, after which at least one periodic orbit nested in A_0 becomes transversely unstable. For example, such threshold has been exceeded when ξ is increased to -0.2964, when the transverse Lyapunov exponent $\Lambda_\perp(\mathcal{O}_4)$ of the period-4 cycle $\mathcal{O}_4$ is positive. This, in turn, implies $\Lambda_\perp^{\max} > 0$ since $\Lambda_\perp(\mathcal{O}_4) \leq \Lambda_\perp^{\max}$. However, at $\xi = -0.2964$, the relation $\Lambda_\perp^{\rm nat} < 0$ holds, that is the chaotic set A_0 is transversely attractive on average and, hence, is a non topological Milnor attractor.

In Fig. 9, displacements r from the attractor A_0 of orbits with initial conditions placed near the synchronization manifold $\mathcal{M}_0$ are displayed versus time. In the simulation presented in the panel (a), chaos synchronization is achieved in the long run after a transient part of the orbit along which the so called on-off intermittency phenomenon is observed (see [3,17,24]). Such a phenomenon corresponds to a sequence of asynchronous bursts, bringing the orbit far from $\mathcal{M}_0$, that are followed by quasi-synchronized states in which the orbit approaches the synchronization manifold $\mathcal{M}_0$.

[3] We recall that $a_0^2q_0 - a_1^2q_1 < 0$.

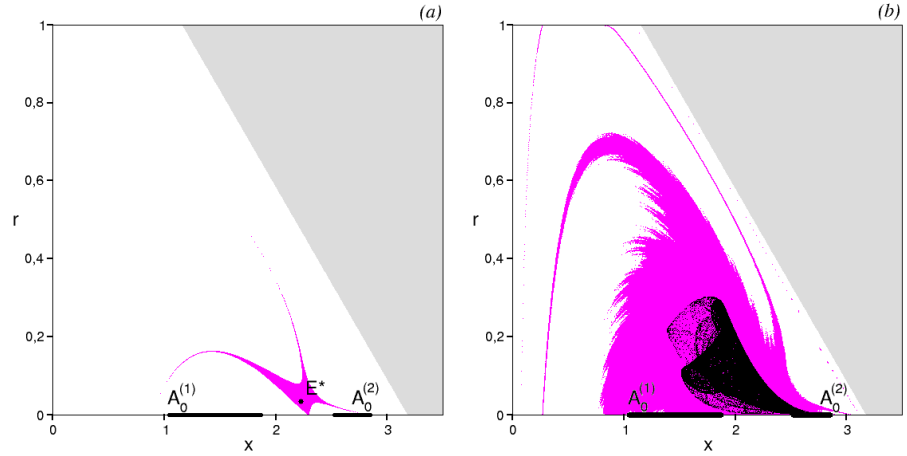

Fig. 8 (a) The asymptotically stable chaotic set A_0 and its basin (white points) coexisting with the stable internal fixed point E^* at $\xi = -0.32$. (b) Riddling between the basin of A_0 and the basin of the internal chaotic attractor at $\xi = -0.2964$. In both simulations, gray points represents the basin of unfeasible orbits. Other parameters are as in Fig. 7.

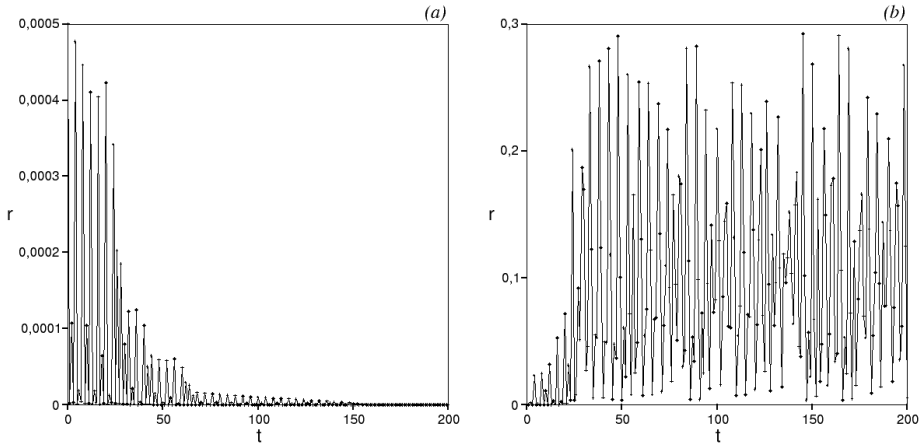

Fig. 9 (a) An orbit with initial condition close to A_0 diverging from A_0 showing the phenomenon of global riddling. Initial condition is placed near $x_0 = 1.2$ and $r = 10^{-5}$. (b) An orbit with initial condition close to A_0 diverging from A_0 showing the phenom of global riddling. Initial condition is placed near the transversely unstable period 4-cycle embedded in A_0. Parameters are as in Fig. 7 and $\xi = -0.2964$.

However, the fate of an orbit starting near $\mathcal{M}_0$ may also be different. This is due to the coexistence of the attractor A_0 with a chaotic inner attractor originated from the fixed point E^* after its loss of stability through Neimark-Sacker bifurcation. This is shown in Fig. 9(b), where an orbit with initial condition placed near the transversely repelling period 4-cycle $\mathcal{O}_4$ nested in A_0 is trapped in the inner chaotic set. Such event can be explained by considering the structure of the basin of attraction of the inner attractor. It shows "tongues" issuing from the Milnor

attractor A_0 that surround the unstable sets of the transversely unstable cycles in A_0 (one of which is the cycle $\mathcal{O}_4$) and their preimages of any rank, which are densely distributed along A_0. In this situation, any neighborhood surrounding the attractor A_0 includes a set of points with positive measure in the plane that belong to the basin of the inner attractor. The basin of A_0 is said to be *globally riddled* with the basin of the inner attractor. Few of such tongues are visible in Fig. 8(b), where the basin of A_0 and the basin of the inner attractor are represented by white and magenta points, respectively, in the phase space.

As the parameter ξ further increases, the natural transverse Lyapunov exponent $\Lambda_{\perp}^{\text{nat}}$ increases as well and global bubbling bifurcation occurs as $\Lambda_{\perp}^{\text{nat}} = 0$. For example, at the value $\xi = -0.295$, the natural transverse Lyapunov exponent $\Lambda_{\perp}^{\text{nat}}$ has just become positive. Then, A_0 in no more a non topological Milnor attractor. However, it is reasonable to conjecture that some cycles nested in A_0 that are transversely attracting are still present. The basin of A_0 is a set of zero Lebesgue measure in the phase space and the long run convergence to synchronization patterns is possible only for non generic initial conditions. In Fig. 10, the basin of the inner attractor is shown in the phase space by magenta points while the basin of attraction of the chaotic saddle A_0 cannot be observed in simulations.

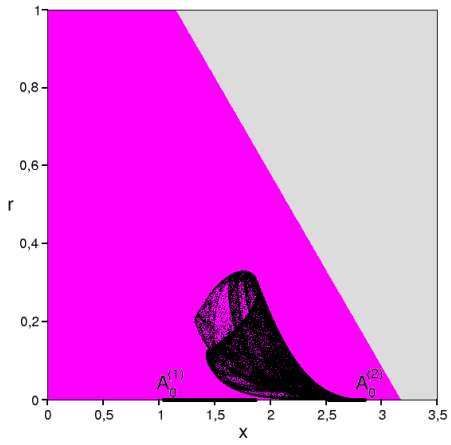

Fig. 10 The transversely repelling chaotic set A_0 characterized by a positive transverse Lyapunov exponent $\Lambda_{\perp}^{\text{nat}}$ coexists with an asymptotically stable internal chaotic attractor at $\xi = -0.295$. Magenta points represent the basin of attraction of the internal attractor while gray points represents the basin of unfeasible orbits. Other parameters are as in figure 7.

We end this section by mentioning that the transverse attractivenes of the attractor A_1 embedded in the synchronization manifold $\mathcal{M}_1$ can be evaluated analogously as it was done for the transverse attractiveness of A_0.

6 Conclusions

By the current work we continue investigating asymptotic behavior of a 2D smooth noninvertible map modeling exploitation of the common renewable resource by

multiple players introduced in [6]. At every time step each player can choose between two strategies, one being more intensive but cheaper and the other one being environmentally friendly but more expensive. The amount of the resource changes according to a quadratic law, which implies that the state space is separated by the critical line into regions Z_0 consisting of points having no preimages and Z_2 containing points with two preimages. Moreover, the boundaries of the domain related to feasible states represent one dimensional invariant manifolds, at which the dynamics is goverened by one dimensional restrictions of the original two dimensional map. These properties entail complex and intriguing dynamic scenarios, among which we focus on those that are not so often encountered in smooth two dimensional systems.

We examine a two particular bifurcation sequences that occur near the flip bifurcation curve of the internal fixed point E^*, revealing coexistence of two internal attractors whose basins of attraction are separated by the stable set of a certain saddle cycle. In addition, for certain parameter values, an 8-piece chaotic attractor is observed, which is associated with a mixed absorbing area confined by segments of critical lines of different rank and segments of unstable sets of two different saddle cycles. Then we also address the problem of synchronization achievement. Namely, we consider an invariant set A_0 located on the boundary $\mathcal{M}_0$ of the feasible domain and investigate its transverse stability by computing its transverse Lyapunov exponents. In other words, we find conditions under which A_0 is attracting not only for the respective one dimensional restriction $f_{r=0}$ but also for the original two dimensional map. We show that, depending on the parameter values, A_0 can be a topological attractor or a weaker Milnor attractor coexisting with another internal attractor. In the former case the boundaries of the corresponding basins are smooth, while in the latter case, the basin of A_0 is globally riddled with the other basin. It means that in an arbitrary neighborhood of any point of A_0, there is a set of points with positive Lebesgue measure belonging to the other basin. Such an occurrence has crucial implications from economic viewpoint, since small perturbations may lead to drastic changes of asymptotic dynamics. This is also an impolrtant discovery for an entire class of evolutionary games that can be modeled by similar kind of maps.

References

1. Abraham, R., Mira, C., Gardini, L.: Chaos in discrete dynamical systems: A visual introduction in 2 dimensions. Springer (1997)
2. Agliari, A., Bischi, G.I., Gardini, L.: Some methods for the global analysis of dynamic games represented by iterated noninvertible maps. In: Oligopoly dynamics, pp. 31–83. Springer (2002)
3. Alexander, J., Yorke, J.A., You, Z., Kan, I.: Riddled basins. Int. J. Bif. Chaos **02**(04), 795–813 (1992). DOI 10.1142/S0218127492000446
4. Antoci, A., Dei, R., Galeotti, M.: Financing the adoption of environment preserving technologies via innovative financial instruments: An evolutionary game approach. Nonlinear Analysis: Theory, Methods & Applications **71**(12), e952 – e959 (2009). DOI https://doi.org/10.1016/j.na.2009.01.077. URL http://www.sciencedirect.com/science/article/pii/S0362546X09000571
5. Ashwin, P., Buescu, J., Stewart, I.: From attractor to chaotic saddle: a tale of transverse instability. Nonlinearity **9**(3), 703–737 (1996). DOI 10.1088/0951-7715/9/3/006
6. Bischi, G.I., Cerboni Baiardi, L., Radi, D.: On a discrete-time model with replicator dynamics in renewable resource exploitation. J. Differ. Equ. Appl. **21**(10), 954–973 (2015)

7. Bischi, G.I., Lamantia, F., Sbragia, L.: Strategic interaction and imitation dynamics in patch differentiated exploitation of fisheries. Ecological Complexity **6**(3), 353–362 (2009). DOI https://doi.org/10.1016/j.ecocom.2009.03.004. URL http://www.sciencedirect.com/science/article/pii/S1476945X0900021X. Special Section: Fractal Modeling and Scaling in Natural Systems
8. Bischi, G.I., Radi, D.: An extension of the antocideigaleotti evolutionary model for environment protection through financial instruments. Nonlinear Analysis: Real World Applications **13**(1), 432–440 (2012). DOI https://doi.org/10.1016/j.nonrwa.2011.07.046. URL http://www.sciencedirect.com/science/article/pii/S1468121811002082
9. Buescu, J.: Exotic Attractors: From Liapunov Stability to Riddled Basins. Birkhauser, Basel (1997)
10. Cabrales, A., Sobel, J.: On the limit points of discrete selection dynamics. Journal of Economic Theory **57**(2), 407–419 (1992). DOI https://doi.org/10.1016/0022-0531(92)90043-H. URL http://www.sciencedirect.com/science/article/pii/002205319290043H
11. Carraro, C., Fragnelli, V.: Game Practice and the Environment. Fondazione Eni Enrico Mattei (FEEM) series on economics and the environment. Edward Elgar Publishing, Incorporated (2004). URL https://books.google.com.ua/books?id=zlvQoL8oEdkC
12. Collet, P., Eckmann, J.: Iterated Maps on the Interval as Dynamical Systems. Springer Science & Business Media, Berlin (2009)
13. Gumovsky, I., Mira, C.: Dynamique Chaotique: Transformations Ponctuelles. Transition Ordre - Dsordre. Collection Nabla. Cépaduès Édition, Toulouse (1980)
14. Hofbauer, J., Sigmund, K.: Evolutionary game dynamics. Bull. Amer. Math. Soc. **40**, 479–519 (2003)
15. Lai, Y.C., Grebogi, C.: Noise-induced riddling in chaotic systems. Phys. Rev. Lett. **77**, 5047–5050 (1996). DOI 10.1103/PhysRevLett.77.5047
16. Lamantia, F., Radi, D.: Exploitation of renewable resources with differentiated technologies: an evolutionary analysis. Math. Comp. Simul. **108**, 155–174 (2015)
17. Maistrenko, Y.L., Maistrenko, V.L., Popovich, A., Mosekilde, E.: Transverse instability and riddled basins in a system of two coupled logistic maps. Phys. Rev. E **57**, 2713–2724 (1998). DOI 10.1103/PhysRevE.57.2713
18. Metropolis, N., Stein, M.L., Stein, P.R.: On finite limit sets for transformations on the unit interval. J. Comb. Theory **A15**, 25–44 (1973)
19. Milnor, J.: On the concept of attractor. Commun. Math. Phys. **99**, 177–195 (1985)
20. Milnor, J.: On the Concept of Attractor, pp. 243–264. Springer New York, New York, NY (1985). DOI 10.1007/978-0-387-21830-4_15
21. Mira, C.: Chaotic Dynamics: From the One-Dimensional Endomorphism to the Two-Dimenaional Diffeomorphism. World Scientific, Singapore (1987)
22. Mira, C., Gardini, L., Barugola, A., Cathala, J.C.: Chaotic Dynamics in Two-Dimensional Noninvertible Maps. Nonlinear Science. World Scientific, Singapore (1996)
23. Nagai, Y., Lai, Y.C.: Periodic-orbit theory of the blowout bifurcation. Phys. Rev. E **56**, 4031–4041 (1997). DOI 10.1103/PhysRevE.56.4031
24. Ott, E., Sommerer, J.C.: Blowout bifurcations: the occurrence of riddled basins and on-off intermittency. Phys. Lett. A **188**(1), 39–47 (1994). DOI https://doi.org/10.1016/0375-9601(94)90114-7
25. Sethi, R., Somanathan, E.: The evolution of social norms in common property resource use. The American Economic Review **86**(4), 766–788 (1996). URL http://www.jstor.org/stable/2118304
26. Sharkovskii, A.N.: Problem of isomorphism of dynamical systems. In: Proc. 5th International Conference on Nonlinear Oscillations, vol. 2, pp. 541–544 (1969)